Available online at www.sciencedirect.com
SCIENCE DIRECT
Surface & Coatings Technology 200 (2006) 6484–6489
SURFACE & COATINGS TECHNOLOGY
www.elsevier.com/locate/surfcoat

Passivation of Al surfaces against oxidation by monoatomic Sn wetting layers

B. Schwarz [a,*], C. Eisenmenger-Sittner [a], E. Klein [a], C. Tomastik [b], K. Mayerhofer [c], P.B. Barna [d], A. Kovács [d]

[a] Vienna University of Technology, Institute of Solid State Physics, A-1040 Wien, Austria
[b] Vienna University of Technology, Institute of General Physics, A-1040 Wien, Austria
[c] Vienna University of Technology, Institute of Chem. Technol. and Analytics, A-1040 Wien, Austria
[d] Research Institute for Technical Physics and Material Science, H-1121 Budapest, Hungary

Available online 9 December 2005

Abstract

Tin (Sn) forms monoatomic wetting layers on aluminium (Al) interfaces under ultra-high vacuum (UHV) conditions. The wetting layer spreads over the Al vacuum interface or over Al grain boundaries via the emergence of Sn atoms from Sn islands. The islands can be generated by sputter-deposition of a 10 nm thick Sn film on a polycrystalline Al underlayer. If the Al/Sn bi-layer is covered by an Al capping layer, Sn will penetrate the capping layer along the grain boundaries and form a wetting layer on its surface. Al surfaces covered by the Sn wetting layer exposed to oxygen (O) are oxidized significantly slower compared to bare Al surfaces. The shape of the adsorption isotherms suggests that the oxidation process involves the formation of oxygen nuclei.

Depositing the Al capping layer in the presence of oxygen leads to a striking effect in the optical appearance and the chemical composition of the capping layer: Light microscopy shows that, in the vicinity of Sn islands, the capping layer has a shiny metallic appearance while the residual areas have a dark colour. By secondary ion mass spectroscopy (SIMS) and transmission electron microscopy (TEM), it could be shown that the dark regions contain significantly more oxygen. This effect can be attributed to the suppression of Al oxidation during the growth of the Al capping layer by the presence of Sn in the vicinity of the Sn islands.

Keywords: Oxidation; Al; Sn; Stranski-Krastanov; Vapour deposition

1. Introduction

The aim of this paper is to better understand the surface processed in the immiscible system of Sn and Al [1], which happens both, during and after deposition. Special emphasis is given to the influence of oxygen impurities on surface processes which can often significantly deviate from expectations based on bulk thermodynamics under atmospheric conditions. Surface alloying of thermodynamically immiscible systems and the formation of pseudomorphic layers on single crystalline substrates during film growth may serve as examples [2–11].

For the present experiments, Al/Sn bi-layers and Al/Sn/Al sandwich layers were produced by physical vapour deposition (PVD) and were investigated by several analytical techniques. For investigating the wetting layer formation [12] and the oxidation of Al/Sn bi-layers, Auger electron spectroscopy (AES) was

Table 1
Deposition parameters

Sputter plant	ALCATEL SCM450, turbomolecular pump
Pumping speed	430 dm^3/s
Base pressure	10^{-5} Pa
Working gas/pressure/measurement	Ar/0.4 Pa/Baratron gauge
Substrate material	Silicon, native oxide
rms-roughness of Si substrate	<1 nm
Distance target/substrate	120 mm
Deposition rate at the substrate: Al	0.5 nm s^{-1}
Layer thickness: Al	400 nm
Deposition rate at the substrate: Sn	0.1 nm s^{-1}
Layer thickness: Sn	10 nm
Deposition temperature: Al/Sn	180 °C

* Corresponding author. Tel.: +43 01 58801 13775; fax: +43 01 58801 13899.
E-mail address: bernhard.schwarz@ifp.tuwein.ac.at (B. Schwarz).

0257-8972/$ - see front matter © 2005 Elsevier B.V. All rights reserved.
doi:10.1016/j.surfcoat.2005.11.027

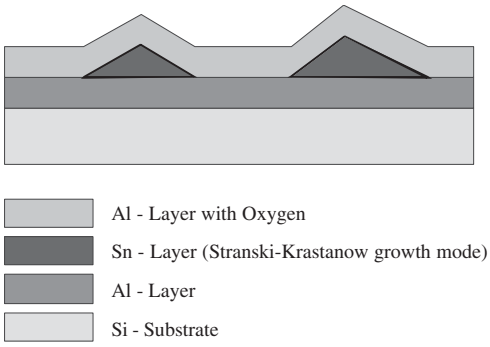

Fig. 1. Schematic cross-section of the Al/Sn/Al sandwich system. The Al capping layer was deposited in the presence of oxygen. The Sn layer appears in a Stranski–Krastanov growth mode. In the case of the Al/Sn bi-layer system, the capping layer was not deposited.

used, while optical micrographs and atomic force microscopy (AFM) images were taken to image the Sn islands resulting from the Stranski–Krastanov growth mode [13]. The effects of oxygen presence in the Al capping layers of Al/Sn/Al systems were investigated by scanning electron microscopy (SEM) and energy dispersive X-ray (EDX) analysis. A more detailed analysis was done by secondary ion mass spectroscopy (SIMS). Cross-sectional transmission electron microscopy (XTEM) was used to image the inner structure of the Al/Sn/Al sandwich layer systems.

This paper is structured as follows: In Section 2, the method of sample preparation and the sandwich structure of the samples themselves are explained; Section 3 gives the results of the different investigation methods; while Section 4 closes with a discussion of the results and gives an outlook on some future work.

2. Experimental

All samples were deposited on Silicon (Si) substrates covered with native oxide. The deposition technique was magnetron sputtering from two separated sputter targets, with the sputter parameters given in Table 1. The layer thicknesses were 400 nm for the Al layer and 10 nm for the Sn layer, both for the Al/Sn and the Al/Sn/Al samples. The substrate temperature was kept constant at 180 °C. The Al capping layer of the sandwich systems was sputtered in the presence of oxygen. In the Al/Sn bi-layer systems, the deposition of Sn was done in different steps, which will be described later.

After sputter deposition, the samples were removed from the vacuum chamber and exposed to the ambient. A schematic cross-section of the Al/Sn/Al sandwich structure is shown in Fig. 1. In the case of the Al/Sn bi-layer system, the Al capping layer was not deposited.

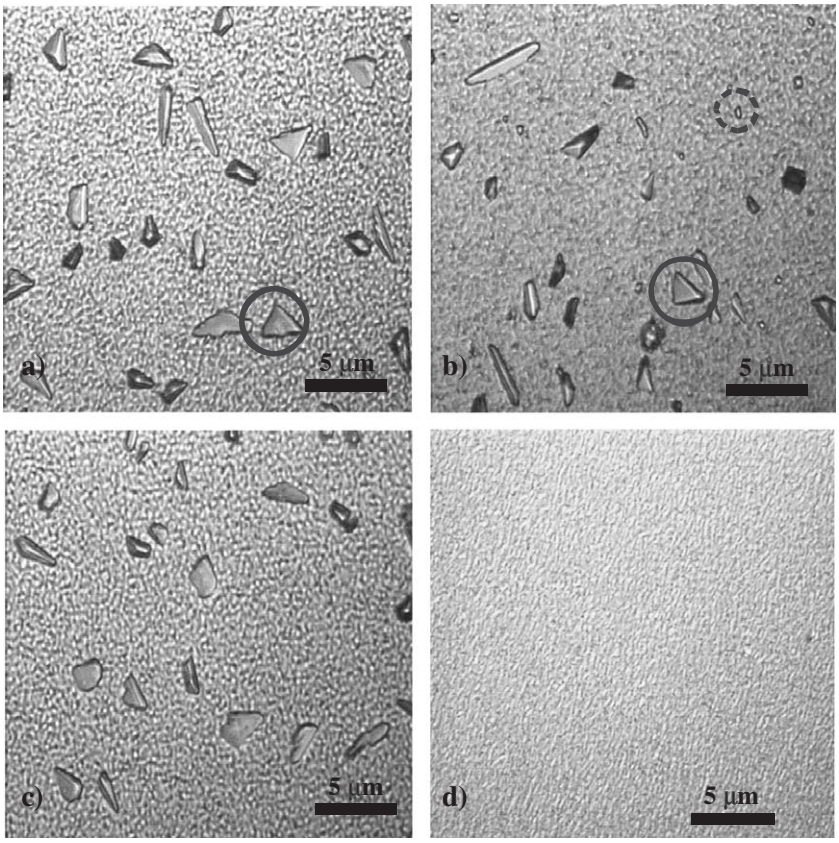

Fig. 2. Optical microscopy images of 4 differently deposited Al/Sn bi-layer samples. (a) Deposition of 10 nm Sn immediately after the Al deposition, Sn islands (full circle) are clearly visible. (b) Al film oxidized 30 min at an oxygen pressure of 2×10^{-4} Pa. Then 10 nm Sn was deposited. Beside large Sn islands (full circle) small islands (dotted circle) are visible. (c) Deposition of 2 nm Sn immediately after the Al deposition; oxidation for 30 min at 2×10^{-4} Pa. Afterwards, deposition of 8 nm Sn. No differences to panel (a) are visible. (d) Al oxidized for 3 min at atmospheric pressure. Then 10 nm Sn were deposited. No Sn islands are visible.

The TEM cross-section samples were mechanically thinned with diamond discs (from 30 μm down to 0.5 μm) to approximately 10 μm followed by ion milling (Gatan PIPS 691 – Precision Ion Polishing System) to electron transparency. The used TEM was a JEOL JEM 200 CX, with a LaB_6 tip and an acceleration voltage of 200 kV. Imaging SIMS measurements were done on an enhanced CAMECA IMS 3f apparatus with Cs^+ as primary ions and negative secondary ions were detected. AFM images were taken with a Topometrix Explorer under atmospheric conditions and the Auger system was a VG Microlab 310F (ultra-high vacuum conditions).

3. Results and discussion

3.1. Al/Sn bi-layer system

This layer system consists of a 400 nm thick Al base layer covered by a 10 nm thick Sn layer. The growth mode of Sn was identified as Stranski–Krastanov type [14], which means that, first, a monoatomic Sn layer is formed on the Al surface followed by 3D island growth. After removing this monoatomic layer via sputter cleaning with Ar ions in the AES chamber under UHV, the wetting layer emerges again from the Sn islands [12]. The wetting layer formation is dependent on impurities present in the Sn island or on the Al surface. The presence of oxygen or carbon in the Sn island inhibits the formation of the wetting layer as shown in [15].

Four different types of Al/Sn bi-layer samples were produced for oxidation experiments. In Fig. 2, optical microscopy images of these four samples are shown. Panel a shows the sample deposited in the absence of oxygen and panel b the Al surface oxidized 30 min at 2×10^{-4} Pa oxygen pressure. Beside the Sn islands, also very small islands appeared. For better visualisation of the two different island types, AFM images were acquired and are shown in Fig. 3. In Fig. 3a, a well-faceted Sn island is visible, contrary to the island in Fig. 3b which is smaller and rounder.

In Fig 2c, 2 nm Sn were deposited prior to the 30 min oxidation at 2×10^{-4} Pa, then the remaining 8 nm Sn were deposited after the oxidation process. No differences to Fig 2a are visible. The Al surface of the sample in Fig. 2d was oxidized for 3 min on atmospheric pressure, then 10 nm Sn were deposited on it. Here no Sn island formation occurs; a continuous layer is formed. The strong oxidation at atmospheric pressure prevents the formation of large Sn islands because of the reduction of the mobility of the Sn atoms.

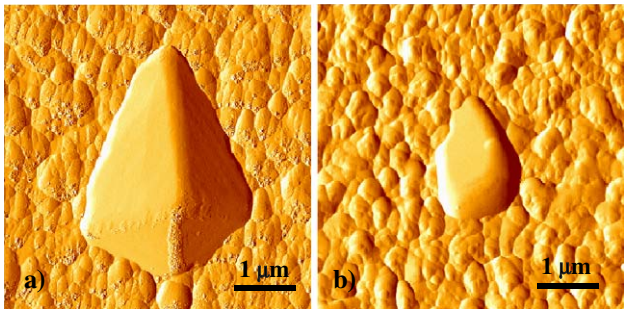

Fig. 3. AFM images of the two different island types: (a) well-faceted Sn island; (b) smaller, rounder Sn island.

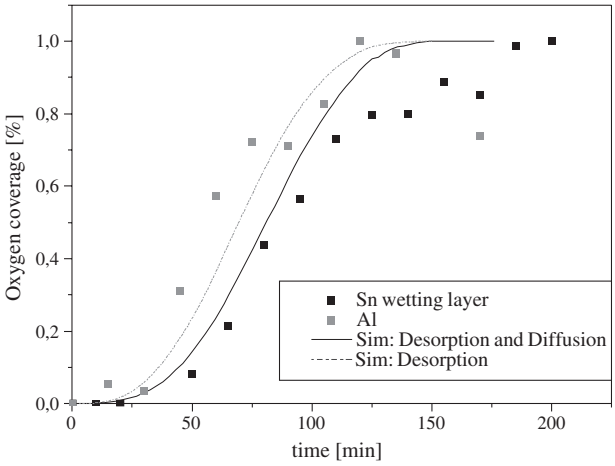

Fig. 4. Comparison of the oxidation of bare Al and Al covered by a Sn wetting layer. A characteristic feature is the delayed start of the oxide growth due to the initial formation of oxide nuclei.

Further oxygen adsorption experiments were done within the AES chamber on a bare Al layer and on a sample with a Sn wetting layer. The surfaces were exposed to an oxygen pressure of 4×10^{-4} Pa which corresponds to an impingement rate of O_2 of 7×10^{-3} monolayers per second. The oxidation process was significantly delayed on the sample which was covered by the Sn wetting layer (Fig. 4).

Moreover, AES spectra from the two different Sn islands types (Fig. 3) were recorded. The spectrum of the large island

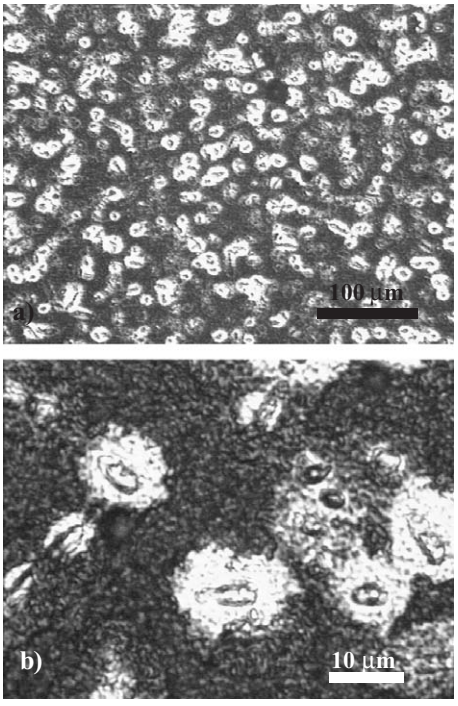

Fig. 5. Optical microscopy images of the Al/Sn/Al sandwich sample. In panels (a) and (b), the sample is shown at 200× and 1500× magnification, respectively. The capped Sn islands, bright halos and dark Al regions between them are visible.

shows no signal beside the Sn peak. The spectrum of the small island shows that it consists of Sn and oxygen. These results in combination with Fig. 2b and Fig. 3b lead to the conclusion that the small islands are decorated oxygen nuclei.

3.2. Al/Sn/Al sandwich layer system

The production routine for the deposition of the Al/Sn/Al sandwich layer systems was as follows: the Al base layer and the Sn layer were sputtered in the same way as the Al/Sn bi-layer samples. The Al capping layer was deposited in the presence of oxygen. The oxygen content was kept at 2% of the Ar content (0.4 Pa) during sputtering, the blank value of the oxygen content in the vacuum chamber was 0.003% (30 ppm). Optical micrographs of the samples are shown in Fig. 5 (magnifications of 200× in panel a and 1500× in panel b). Three different regions can be distinguished: the overgrown Sn islands, a bright halo around the Sn islands and a residual dark area.

For the chemical investigation of these samples, EDX measurements were carried out on the three different surface areas. The oxygen distribution of the samples was investigated by Imaging SIMS. Fig. 6 shows a SEM image, where different surface morphologies are clearly visible. EDX spectra were taken from these three different regions, and the results of the measurements are summarized in Table 2. The spectra of the Sn island and the Sn halo are also shown in the top of Fig. 6. The high Sn content in the Sn island was as expected, but the halo around the island also contains a certain amount of Sn. In the dark region between the islands,

Table 2
This table shows the elemental concentration in the three different surface regions of the oxidized Al/Sn/Al sample

	Element	at.%
Sn – island	Sn	2.8
	Al	82.6
	O	14.6
Sn – halo	Sn	0.7
	Al	84.6
	O	14.7
Al – area	Sn	0.1
	Al	74.0
	O	25.8

There was only one measurement taken for an overview, so no standard deviation could be given.

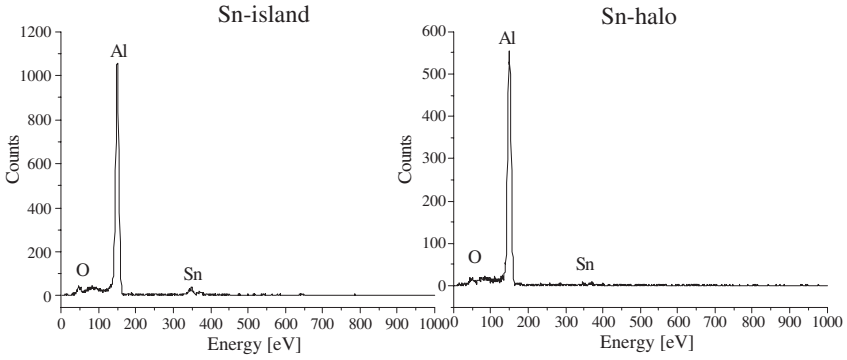

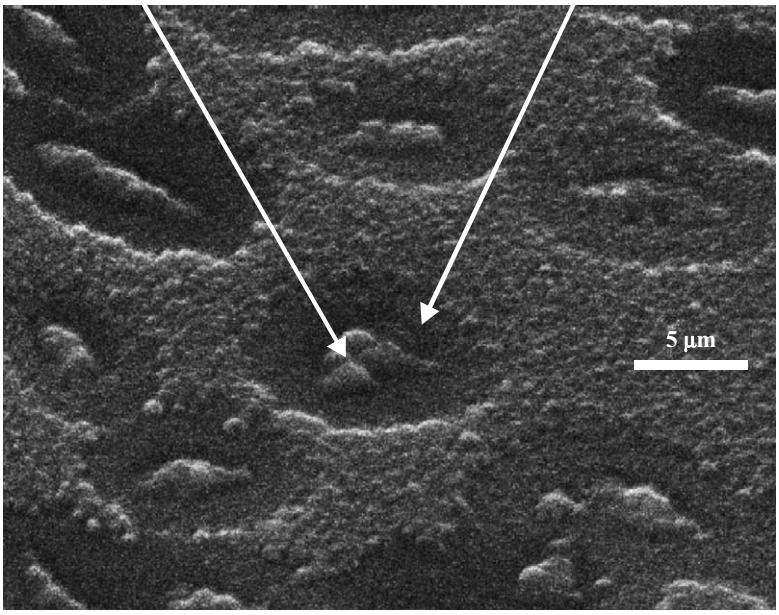

Fig. 6. SEM image of the Al/Sn/Al sample. Here the three different surface types, Sn islands, Sn halos and dark Al region between, are also visible. The EDX spectra from the Sn island and the Sn halo are above shown. The Sn content in the Sn island is clearly visible but also in the Sn halo was a detectable Sn signal (see Table 2).

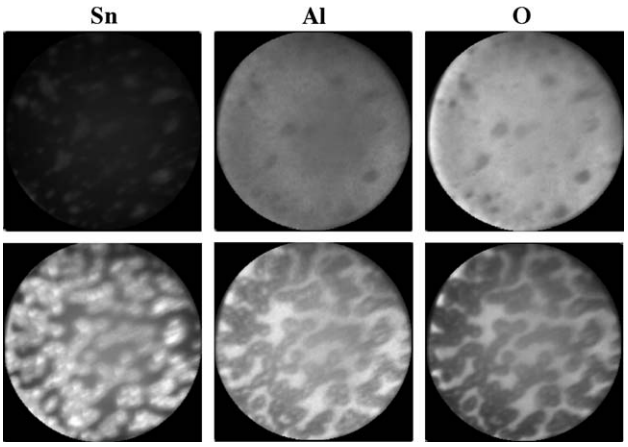

Fig. 7. SIMS images of the Al/Sn/Al sample. The elemental mapping for Sn, Al and oxygen is given: (top) just beneath the surface; (below) in the middle of the Al capping layer.

the Sn content is close to zero. Because of contaminations of the surface, the oxygen content measured by EDX is not reliable; although, a tendency of a higher oxygen content within the dark areas exists. For a more accurate measurement, SIMS was used because surface contaminations are removed in the chamber during this analysis. For oxygen, the matrix effect of this method is very low, so the oxygen amount can be determined very accurately.

Fig. 7 gives a summary of SIMS images taken during the analysis of the sample. Bright regions correspond to higher elemental concentration. In the Sn column, one can see that Sn is already near the surface detectable and with greater depth Sn islands and their halos are distinguishable. This is in agreement with the EDX spectra. Oxygen signals and Al signals coincide during the whole image series which leads to the conclusion that the dark regions of the optical microscopy images are aluminium oxide. Sn signals and Al (and oxygen) signals are always in opposite to each other. So the presence of Sn atoms in the halos of the Sn islands is responsible for the suppression of Al oxidation during the film growth of the Al capping layer.

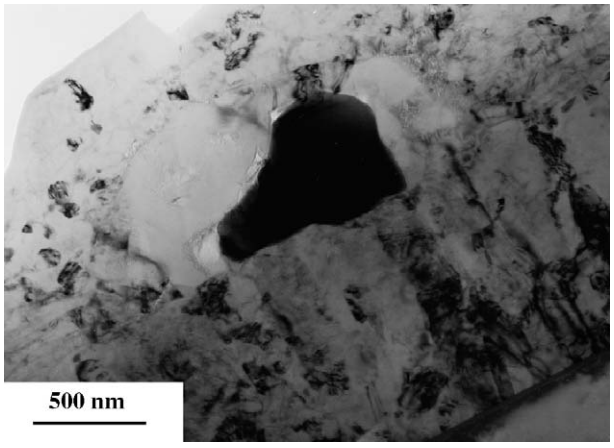

Fig. 8. XTEM image of the Al/Sn/Al sandwich system. The Al base layer, the Sn island and the Al capping layer are visible in this image. The interface between the two Al layers is also in the vicinity of the Sn island clearly visible.

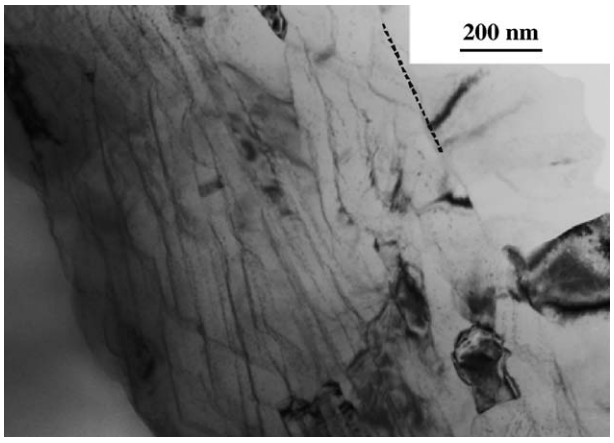

Fig. 9. XTEM image of the Al capping layer. The interface to the Al base layer is additionally marked by the dotted line. In the oxidized Al capping layer, many growth lamellae are visible.

XTEM was performed to get structural information of the Al/Sn/Al sandwich layer system. In Fig. 8, all three layers visible: Al base layer, Sn layer (island) and oxidized Al capping layer. The base layer has a polycrystalline structure of columnar grains in accordance with several structure zone models [16–18]. The oxidized Al capping layer in a higher magnification is shown in Fig. 9. The interface between the two Al layers is marked by the dotted line in the image. One can clearly recognise a lamellar structure within the capping layer. This growth mechanism is explained in detail in Eisenmenger-Sittner et al. [19]. In comparison to that reference, where the lamellae appeared in the capping layer without the intentional addition of oxygen, the present lamellae appeared to be more pronounced (higher contrast).

4. Conclusion and outlook

In this work, the oxidation behaviour of the Al/Sn bi-layer and Al/Sn/Al sandwich systems was investigated. For the bi-layer systems, it was found that the presence of Sn inhibits the oxidation of Al surfaces. For the sandwich systems, the presence of oxygen during the deposition of the capping layer resulted in the formation of Sn halos with a lower oxygen content than in the surrounding coating regions. This can be attributed to the presence of Sn in the vicinity of the Sn islands which can be transported a short distance by grain boundary diffusion. XTEM additionally showed a lamellae growth mode in the oxidized Al capping layer.

Future investigations will be performed at different substrate temperatures and oxygen partial pressures to study the correlation of these two parameters.

Acknowledgement

This work is supported by the Austrian Science Fund (FWF) under grant no. P-15739. The TEM investigations were performed in collaboration with the University Service Center for Transmission Electron Microscopy (USTEM) of the Vienna University of Technology.

References

[1] T.B. Massalski, Binary Alloy Phase Diagrams, vol. 2, ASM International, The Materials Society, Metals Park, 1990.
[2] M. Michailow, C. de Beauvais, D. Rouxel, B. Mutaftschiew, Phys. Rev., B 61 (9) (2000) 5987.
[3] G.L. Kellog, R.A. Plass, Surf. Rev. Lett. 7 (5–6) (2000) 649.
[4] G. Prevot, C. Cohen, J.M. Guigner, D. Schmaus, Phys. Rev., B 61 (15) (2000) 10393.
[5] G. Vidali, Hong Zeng, Appl. Surf. Sci. 92 (1996) 11.
[6] C. Nagl, E. Platzgummer, M. Schmid, P. Varga, S. Speller, W. Heiland, Phys. Rev. Lett. 75 (16) (1995) 2976.
[7] C. Argile, G.E. Rhead, Surf. Sci. 78 (1978) 125.
[8] C. Argile, G.E. Rhead, Thin Solid Films 67 (1980) 299.
[9] K. Gürtler, K. Jakobi, Surf. Sci. 134 (1983) 309.
[10] M. Jiang, M. Quiu, Y.J. Zhao, P.L. Cao, Phys. Lett., A 239 (1998) 127.
[11] D. Bimberg, M. Grundmann, N.N. Ledentsov, S.S. Ruvimow, P. Werner, U. Richter, J. Heydenreich, V.M. Ustinov, P.S. Kop'ev, Thin Solid Films 267 (1995) 32.
[12] C. Eisenmenger-Sittner, H. Bangert, A. Bergauer, J. Brenner, H. Störi, P.B. Barna, Vacuum 71 (2003) 253.
[13] C. Eisenmenger-Sittner, H. Bangert, H. Störi, J. Brenner, P.B. Barna, Surf. Sci. 489 (2001) 161.
[14] C. Argile, G.E. Rhead, Surf. Sci. Rep. 10 (1989) 277.
[15] E. Klein, B. Schwarz, C. Eisenmenger-Sittner, C. Tomastik, P.B. Barna, A. Kovács, Vacuum 80 (2005) 74.
[16] J.A. Thornton, J. Vac. Sci. Technol. 11 (4) (1974) 666.
[17] J.A. Thornton, J. Vac. Sci. Technol. 12 (4) (1975) 830.
[18] S. Graig, G.L. Harding, J. Vac. Sci. Technol. 19 (2) (1981) 205.
[19] C. Eisenmenger-Sittner, H. Bangert, C. Tomastik, P.B. Barna, A. Kovács, F. Misiak, Thin Solid Films 433 (2003) 97.